Response Surface Methodology Study on Magnetite Nanoparticle Formation under Hydrothermal Conditions

Regular Paper

Naoya Mizutani[1], Tomohiro Iwasaki[1*] and Satoru Watano[1]

1 Department of Chemical Engineering, Osaka Prefecture University, Osaka, Japan
* Corresponding author(s) E-mail: iwasaki@chemeng.osakafu-u.ac.jp

Abstract

In a hydrothermal preparation of crystalline magnetite (Fe_3O_4) nanoparticles, the influence of the experimental parameters (initial molar ratio of ferrous/ferric ions, initial concentration of ferrous ions, and heating time), and their interactions, on the particle formation was studied using response surface methodology (RSM), based on a statistical design of experiments (DOE). As indices indicating particle formation and crystallization, the variation in the particle diameter and crystallite size with the synthesis conditions was examined. The crystallite size was greatly affected by both the initial ferrous/ferric ion molar ratio and the heating time, whereas the particle diameter strongly depended on the heating time, and on the interaction between the initial ferrous/ferric ion molar ratio and the initial concentration of ferrous ions. The results from a statistical analysis suggest that the polycrystalline Fe_3O_4 nanoparticles form via crystal growth and/or thermal aggregation, after nucleation during hydrothermal treatment.

Keywords magnetite nanoparticles, hydrothermal synthesis, response surface methodology, particle growth mechanism

1. Introduction

Nanometre-sized magnetic materials have received intensive attention because of their vital applications in numerous areas, such as ferrofluids, medical diagnostics, advanced magnetic materials, and catalysts [1–4]. In particular, magnetite (Fe_3O_4) nanoparticles are useful because of their potential in biomedical applications [5] (e.g., magnetic resonance imaging [6] and targeted drug delivery [7]). Various methods of preparing Fe_3O_4 nanoparticles have been developed [8]. Among them, liquid-phase synthesis methods, such as micro-emulsion [9], thermal decomposition of iron complex in organic solvent [10], and co-precipitation of ferrous ions and ferric ions in alkaline medium [11,12], are effective for obtaining Fe_3O_4 nanoparticles relatively easily. Notably, the hydrothermal technique can provide highly crystalline Fe_3O_4 nanoparticles with good magnetic properties, because the Ostwald ripening allows for crystal growth [13].

During the hydrothermal preparation, the formation of Fe_3O_4 nanoparticles is sensitive to the synthesis conditions – such as the reaction time, temperature, and concentration of the reactive species – since the activity of reactants can increase under hydrothermal conditions [14,15]. In our previous studies, we have experimentally investigated the

size control of Fe_3O_4 nanoparticles under various hydro-thermal conditions and found some interesting results [16–18]. For example, the iron hydroxides as a precursor of Fe_3O_4 were not co-precipitated, but sequentially precipitated to control the supersaturation and then hydrothermally heated, which demonstrated that the formation of iron hydroxides was one of the most important factors affecting the size of resultant Fe_3O_4 nanoparticles [18]. Therefore, to precisely control the crystal growth of Fe_3O_4 nanoparticles under proper conditions, the influence of hydrothermal conditions on particle formation must be fully understood. However, the details have so far remained unclear.

One powerful tool for analysing the degree of the effect of each experimental parameter is response surface methodology (RSM), based on a statistical design of experiments (DOE), which can lead to the optimization of synthesis conditions. A number of studies have applied the RSM approach to analyse the preparation of Fe_3O_4 nanoparticles. Forge et al. employed RSM to optimize the synthesis conditions in a co-precipitation method using aqueous and organic media, and determined the important factors for controlling the particle size in each medium [11]. To the best of our knowledge, however, the application of RSM to the modelling and analysis of hydrothermal synthesis has not yet been reported.

For this paper, the influence of the experimental parameters of a hydrothermal preparation of Fe_3O_4 nanoparticles on particle formation was studied using RSM. We focused on the variation in the particle diameter and crystallite size as indices for particle formation and crystallization under the synthesis conditions. Based on the results obtained using the statistical analysis method, the experimental parameters suitable for precisely controlling the particle formation are discussed.

2. Experimental

All chemicals of analytical reagent grade were purchased from Wako Pure Chemical Industries and used as received without further purification. Crystalline Fe_3O_4 nanoparticles were hydrothermally synthesized after co-precipitation of ferrous and ferric ions at room temperature. Predetermined amounts of ferrous sulphate ($FeSO_4$) and ferric chloride ($FeCl_3$) were dissolved in 40 mL of deionized and deoxygenated water in a stainless steel autoclave. In total, 20 mL of 1 $kmol/m^3$ sodium hydroxide (NaOH) solution was added to the solution at a constant rate of 3 mL/min, under vigorous stirring with a magnetic stirrer in an argon atmosphere. The amount of NaOH added was excessive to the stoichiometric formation of iron hydroxides – $Fe(OH)_2$ and $Fe(OH)_3$ – to ensure that the pH value of the solution was higher than 13. Fe_3O_4 forms according to the following chemical reaction, which indicates that an initial Fe^{2+}/Fe^{3+} ion molar ratio of 0.5 is stoichiometrically required for Fe_3O_4 to form:

$$FeSO_4 + 2FeCl_3 + 8NaOH \qquad (1)$$
$$\rightarrow Fe_3O_4 + Na_2SO_4 + 6NaCl + 4H_2O$$
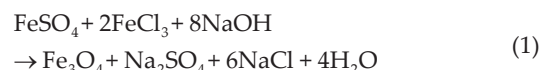
In this study, however, the initial Fe^{2+}/Fe^{3+} ion molar ratio was varied to alter the crystal growth of Fe_3O_4. After the air in the autoclave was replaced with argon to prevent oxidation, the sealed autoclave was maintained at 120°C in an oven, for a given heating time. The product was washed with deionized and deoxygenated water, and dried overnight under a vacuum at 30°C.

To model and evaluate the influence of synthesis conditions on the Fe_3O_4 nanoparticle formation, three independent variables – namely, the initial Fe^{2+}/Fe^{3+} ion molar ratio, initial concentration of Fe^{2+} ions before addition of the NaOH solution, and heating time (denoted as A, B, and C, respectively) – were employed as the representative parameters. The experiments were designed using a central composite design (CCD) [19], which consisted of eight corners and one centre point of the cubic region, and two repetitions. Table 1 summarizes the levels and ranges of independent variables. The plus and minus signs indicate the upper and lower limits of each range, respectively. The zero corresponds to the centre point. Based on our previous study [16], the independent variables were determined as follows: A was varied from 0.5 to 2.0 by adjusting the amount of $FeCl_3$ under a given $FeSO_4$ concentration, and B and C were varied from 16.7 to 33.3 mol/m^3 and from 1 to 20 h, respectively. The experiments of Run No. 10 and 11 were performed to confirm the reproducibility. To minimize unexpected errors, the order of experiments was randomized.

The powder X-ray diffraction (XRD) patterns of the products were measured with CuKα radiation ranging from 2θ=10 to 80°, at a scanning rate of 1°/min, using a Rigaku RINT-1500 powder X-ray diffractometer. The lattice constant was also determined as being between 0.838 nm and 0.841 nm from diffraction angles that exhibited high intensity peaks, which was closer to the standard value of Fe_3O_4 (0.840 nm) than that of maghemite (0.835 nm). The XRD analysis confirmed that the products had a single phase of Fe_3O_4 in all synthesis conditions. The average crystallite size was calculated from the full-width at half-maximum (FWHM) of the (311) diffraction peak of Fe_3O_4 observed at 2θ=35.5° using Scherrer's formula. The hydrodynamic size distributions (number basis) were measured by dynamic light scattering (DLS; Zetasizer Nano ZS, Malvern Instruments) for the colloidal solutions of well-dispersed nanoparticles by ultrasonication, and the median particle diameter was determined. Magnetic properties (i.e., magnetization hysteresis cycle) were analysed using a superconducting quantum interference device (SQUID) magnetometer (MPMS XL, Quantum Design) at 300 K, over a magnetic field range of –10 kOe to 10 kOe.

Run No.	Levels			Conditions		
	A	B	C	A	B [mol/m³]	C [h]
1	–	–	–	0.5	16.7	1
2	0	0	0	1.25	25.0	10.5
3	+	–	+	2.0	16.7	20
4	+	+	–	2.0	33.3	1
5	–	+	+	0.5	33.3	20
6	+	–	–	2.0	16.7	1
7	–	+	–	0.5	33.3	1
8	–	–	+	0.5	16.7	20
9	+	+	+	2.0	33.3	20
10	+	+	+	2.0	33.3	20
11	+	+	+	2.0	33.3	20

Notes: A = initial Fe^{2+}/Fe^{3+} ion molar ratio, B = initial concentration of Fe^{2+} ions, and C = heating time

Table 1. Levels of independent variables and experimental conditions

3. Results and Discussion

Table 2 lists the crystallite size and particle diameter of Fe_3O_4 nanoparticles obtained under each synthesis condition. To analyse the degree of the effect of each experimental parameter and their interactions on the crystallite size and particle diameter, an analysis of variance (ANOVA), based on a linear statistical model, was applied. First, the sum of squares was calculated from the experimental results, using commercially available software (Design-Expert, version 7.1.5, Stat-Ease). Then, the p-value was determined using the sum of squares and the degrees of freedom. The p-value indicates the probability used to determine statistically significant effects in the model. A p-value close to zero indicates that the effect of the experimental parameter is significant; however, if a p-value is larger than 0.1, then the effect is not significant.

The p-values were calculated for various combinations of experimental parameters. In the ANOVA for the crystallite size, when A, B, C, AB and BC were selected (where AB and BC indicate the interactions between A and B, and between B and C, respectively), their p-values were in the lowest level compared to those for other combination sets (Table 3). The significant factors affecting the crystallite size can be determined based on a comparison between the p-values. According to Table 3, A showed the lowest p-value and C the second lowest. However, the interactions between A and B and between B and C were relatively small, and the effect of B was the smallest among the factors. Therefore, the order of efficacy of the factors on the crystallite size was found

to be A > C > BC > AB > B. This result implies that A is the most important factor in obtaining Fe_3O_4 nanoparticles with high crystallinity.

Run No.	Average crystallite size [nm]	Median particle diameter [nm]
1	13.5	30.1
2	20.0	32.7
3	30.7	31.4
4	21.0	36.1
5	17.7	32.4
6	20.4	26.0
7	17.4	27.4
8	20.0	36.7
9	24.6	43.6
10	22.5	45.8
11	22.6	43.0

Table 2. Crystallite size and particle diameter of products

Source	Degree of freedom	Sum of squares	p-value
A	1	102.65	0.0005
B	1	3.25	0.2087
C	1	54.34	0.0020
AB	1	8.97	0.0618
BC	1	26.60	0.0091

**Table 3.** ANOVA results for the crystallite size

In addition to the ANOVA, a polynomial model including interactions and quadratic terms was generated for all response variables, by using a multiple linear regression analysis (MLRA) approach [20,21] to construct the three-dimensional surface plot. A general form of the MLRA model can be represented as follows:

$$Y = \beta_0 + \beta_1 A + \beta_2 B + \beta_3 C + \beta_4 AB + \beta_5 BC + \beta_6 CA + \beta_7 A^2 + \beta_8 B^2 + \beta_9 C^2 + \beta_{10} ABC \tag{2}$$

where β_0 is the intercept representing the arithmetic average of all quantitative outcomes of 11 runs; β_1 to β_{10} are the coefficients computed from the observed experimental values of the crystallite size Y; and A, B and C are the coded levels of the independent variables. The three-dimensional surface plots of the crystallite size versus A and C are shown in Figure 1, generated by the Design-Expert software. The response was represented by an increasing surface with increases of A and C. The obtained surface suggests that the crystallites gradually grow using the surplus $Fe(OH)_2$ at high A regardless of B, which may be attributed to the Schikorr reaction [22]:

$$3Fe(OH)_2 \rightarrow Fe_3O_4 + H_2 + 2H_2O \qquad (3)$$
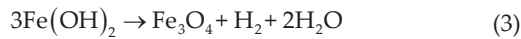
When B was high, however, the crystallite size varied slightly with variations in A and C when compared to the case of low B; nucleation rapidly occurred at high B, which might have reduced the effect of the crystal growth using surplus $Fe(OH)_2$.
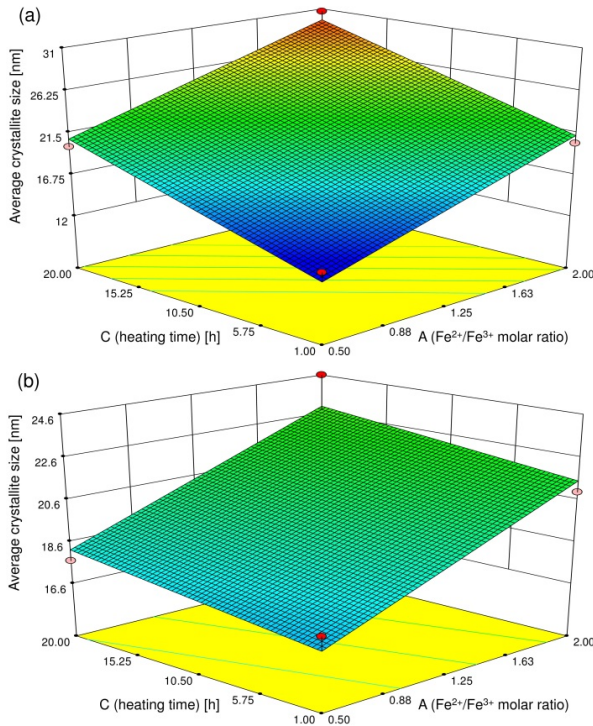
Figure 1. Three-dimensional surface plots for average crystallite size in initial Fe^{2+} ion concentrations (B) of (a) 16.7 mol/m^3 and (b) 33.3 mol/m^3

Subsequently, using the particle diameter data, the particle formation was analysed in an identical manner as described above. In this analysis, the smallest *p*-values were obtained when A, B, C, and AB were used (Table 4). The order of efficacy of the factors on the particle diameter was found to be AB > C > B > A. In contrast to its effect on crystallite size, the interaction between A and B was confirmed to have a large effect on particle diameter. Table 2 demonstrates that the particle diameter was larger than the crystallite size in all products, indicating that the Fe_3O_4 nanoparticles were polycrystalline. Thus, we can conclude that the size of Fe_3O_4 nanoparticles can increase under hydrothermal conditions not only as a result of crystal growth from the nuclei, but of thermal aggregation as well. Accordingly, particle formation by aggregation may be affected by the interaction between A and B.

Figure 2 shows the three-dimensional surface plots of the particle diameter versus A and C. A showed a large effect at high B, which was a similar result to that found for the crystallite size, shown in Figure 1. However, at low B, C had a remarkably large effect on the particle diameter. When B

was low, even at high A the amount of surplus $Fe(OH)_2$ was relatively small, resulting in a low effect of the crystal growth on the particle formation. By contrast, when both A and B were low, the surplus $Fe(OH)_2$ had little effect and the Fe_3O_4 nanoparticles grew rapidly, via the thermal aggregation of Fe_3O_4 and/or iron hydroxides forming as a result of co-precipitation. When both A and B were high, however, the remarkable crystal growth of Fe_3O_4 nanoparticles might have occurred due to the surplus $Fe(OH)_2$.

Source	Degree of freedom	Sum of squares	*p*-value
A	1	19.83	0.0084
B	1	39.12	0.0016
C	1	94.23	0.0002
AB	1	132.44	<0.0001

Table 4. ANOVA results for the particle diameter
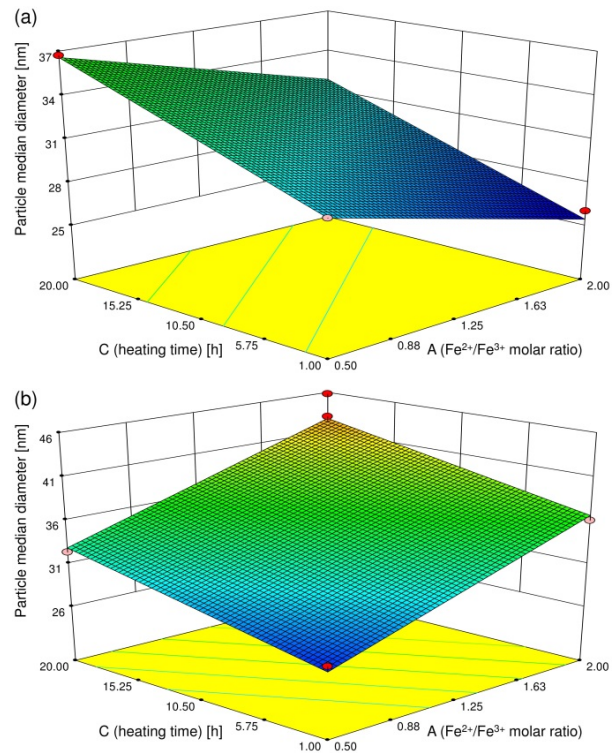
Figure 2. Three-dimensional surface plots for median particle diameter in initial Fe^{2+} ion concentrations (B) of (a) 16.7 mol/m^3 and (b) 33.3 mol/m^3

The results above suggest that polycrystalline Fe_3O_4 nanoparticles formed under hydrothermal conditions according to a possible mechanism that mainly consists of two phenomena – crystal growth and thermal aggregation – which varies remarkably depending on the synthesis conditions (in particular, the amount of ferrous ions). Therefore, we can conclude that the initial Fe^{2+}/Fe^{3+} ion molar ratio (A) is one of the most important factors affecting the formation of Fe_3O_4 nanoparticles. In this paper, A was greatly varied from 0.5 to 2.0 according to the central

composite design. Thus, experiments where A is varied by smaller amounts might lead to more detailed information relating to the crystal growth mechanism [16]. This analysis will be our future work and the results will be reported elsewhere.

Table 5 lists the saturation magnetization and coercivity of the products. Although the saturation magnetization values were lower than that of the corresponding bulk (92 emu/g) due to their smaller size, the products had a relatively high saturation magnetization compared with maghemite nanoparticles with a crystallite size similar to that of the products [23]. This suggests that the products are pure Fe_3O_4. In general, the magnetization tends to vary depending on the crystallinity. However, the saturation magnetization per unit mass obtained in this study shows no clear tendency, as the saturation magnetization is not so greatly affected by the crystallite size [24]. Furthermore, the products may contain a tiny amount of adsorbed water even after drying, which can increase the variation of the magnetization. Thus, the ANOVA for the saturation magnetization data showed no clear correlation with the experimental parameters, or their interactions. Therefore, using the coercivity data, the effect of the factors on the magnetic properties was analysed. After the p-values were calculated for various combinations of factors, the significant factors affecting the coercivity were determined to be A, B, C, and AC, and the order of efficacy was C > AC > A > B, as shown in Table 6.

Run No.	Saturation magneti-zation [emu/g]	Coercivity [Oe]
1	59.9	21.5
2	71.6	81.6
3	60.2	74.3
4	69.4	74.0
5	66.5	97.8
6	59.7	74.3
7	56.0	44.2
8	69.0	71.3
9	54.8	74.4
10	66.6	107.8
11	71.2	80.3

Table 5. Magnetic properties of products

Figure 3 shows the three-dimensional surface plots of the coercivity versus A and C. As with the crystallite size (Figure 1), A and C both had a large effect on the coercivity, which was independent of B. When A and C were increased at low C and low A, respectively, the coercivity greatly increased due to increases in the crystallite size. However, when A and C were high, variation in the coercivity was slight. In general, the Fe_3O_4 nanoparticles with a crystallite size smaller than approximately 20–30 nm have a single-domain structure, and their coercivity increases when the crystallite size increases. However, as the crystallite size

increases further, the magnetic domain structure changes from single-domain to multi-domain, resulting in a decrease in the coercivity [25]. Our products with relatively large average crystallite sizes can consist of both the single-domain and multi-domain Fe_3O_4 nanoparticles, which may lead to a slight variation in the coercivity.

Source	Degree of freedom	Sum of squares	p-value
A	1	752.15	0.0800
B	1	499.93	0.1370
C	1	1846.09	0.0165
AC	1	1199.63	0.0376

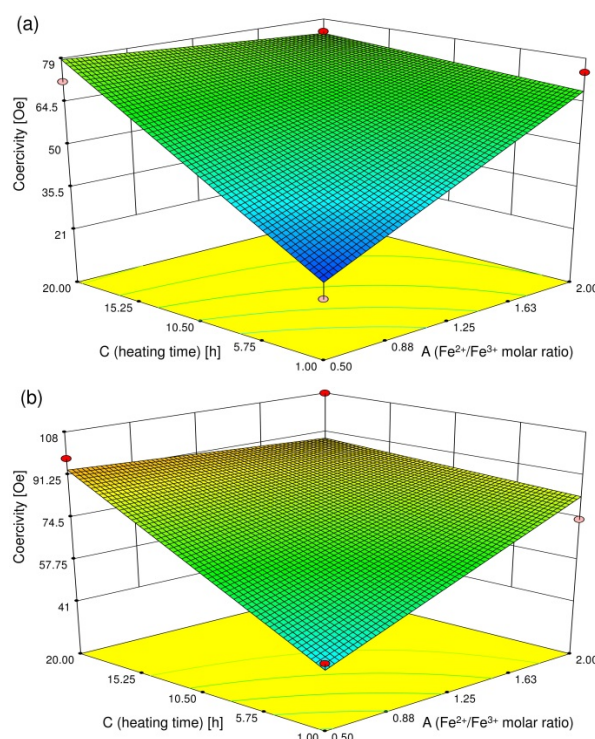Table 6. ANOVA results for the coercivity

Figure 3. Three-dimensional surface plots for coercivity in initial Fe^{2+} ion concentrations (B) of (a) 16.7 mol/m^3 and (b) 33.3 mol/m^3

4. Conclusions

The hydrothermal synthesis of crystalline Fe_3O_4 nanoparticles was performed under different conditions of initial Fe^{2+}/Fe^{3+} ions molar ratios (A), initial Fe^{2+} ion concentrations (B) and heating time (C), to investigate the influence of experimental parameters on particle formation. The order of efficacy of the effective factors on the crystallite size was A > C > BC > AB > B, whereas the order for particle diameter was AB > C > B > A. This result implies that the formation of polycrystalline Fe_3O_4 nanoparticles progresses according to two phenomena – i.e., crystal growth and thermal aggregation – and is greatly affected by the synthesis conditions. The coercivity was closely correlated with A

Naoya Mizutani, Tomohiro Iwasaki and Satoru Watano: Response Surface Methodology Study on Magnetite Nanoparticle Formation under Hydrothermal Conditions

5

and C as well as the crystallite size. The dependence of the coercivity on the crystallite size was explained by the change in the magnetic domain structure. Consequently, the three parameters we employed were found to be important factors in the control of particle formation affecting magnetic properties.

5. References

[1] López-López MT, Durán JDG, Delgado AV, González-Caballero F (2005) Stability and magnetic characterization of oleate-covered magnetite ferrofluids in different nonpolar carriers. J. Colloid Interf. Sci. 291: 144–151.

[2] Bulte JWM, Kraitchman DL (2004) Iron oxide MR contrast agents for molecular and cellular imaging. NMR Biomed. 17: 484–499.

[3] Liao ZM, Li YD, Xu J, Zhang JM, Xia K, Yu DP (2006) Spin-filter effect in magnetite nanowire. Nano Lett. 6: 1087–1091.

[4] Weiss W, Ranke W (2002) Surface chemistry and catalysis on well-defined epitaxial iron-oxide layers. Prog. Surf. Sci. 70: 1–151.

[5] Rajendran R, Muralidharan R, Gopalakrishnan RS, Chellamuthu M, Ponnusamy SU, Manikandan E (2011) Controllable synthesis of single-crystalline Fe_3O_4 nanorice by a one-pot, surfactant-assisted hydrothermal method and its properties. Eur. J. Inorg. Chem. 2011: 5384–5389.

[6] Tian Y, Yu B, Li X, Li K (2011) Facile solvothermal synthesis of monodisperse Fe_3O_4 nanocrystals with precise size control of one nanometre as potential MRI contrast agents. J. Mater. Chem. 21: 2476–2481.

[7] Chen FH, Zhang LM, Chen QT, Zhang Y, Zhang ZJ (2010) Synthesis of a novel magnetic drug delivery system composed of doxorubicin-conjugated Fe_3O_4 nanoparticle cores and a PEG-functionalized porous silica shell. Chem. Commun. 46: 8633–8635.

[8] Teja AS, Koh PY (2009) Synthesis, properties, and applications of magnetic iron oxide nanoparticles. Prog. Cryst. Growth Charact. Mater. 55: 22–45.

[9] Gotić M, Jurkin T, Musić S (2007) Factors that may influence the micro-emulsion synthesis of nanosize magnetite particles. Colloid Polym. Sci. 285: 793–800.

[10] Sun S, Zeng H (2002) Size-controlled synthesis of magnetite nanoparticles. J. Am. Chem. Soc. 124: 8204–8205.

[11] Forge D, Roch A, Laurent S, Tellez H, Gossuin Y, Renaux F, Elst LV, Muller RN (2008) Optimization of the synthesis of superparamagnetic contrast agents by the design of experiments method. J. Phys. Chem. C 112: 19178–19185.

[12] Wang X, Zhang C, Wang X, Gu H (2007) The study on magnetite particles coated with bilayer surfactants. Appl. Surf. Sci. 253: 7516–7521.

[13] Sugimoto T (2003) Formation of monodispersed nano- and micro-particles controlled in size, shape, and internal structure. Chem. Eng. Technol. 26: 313–321.

[14] Ahmadi S, Chia CH, Zakaria S, Saeedfar K, Asim N (2012) Synthesis of Fe_3O_4 nanocrystals using hydrothermal approach. J. Magn. Magn. Mater. 324: 4147–4150.

[15] Ozel F, Kockar H (2015) Growth and characterizations of magnetic nanoparticles under hydrothermal conditions: reaction time and temperature. J. Magn. Magn. Mater. 373: 213–216.

[16] Mizutani N, Iwasaki T, Watano S, Yanagida T, Tanaka H, Kawai T (2008) Effect of ferrous/ferric ions molar ratio on reaction mechanism for hydrothermal synthesis of magnetite nanoparticles. Bull. Mater. Sci. 31: 713–717.

[17] Mizutani N, Iwasaki T, Watano S, Yanagida T, Kawai T (2010) Size control of magnetite nanoparticles in hydrothermal synthesis by coexistence of lactate and sulfate ions. Curr. Appl. Phys. 10: 801–806.

[18] Iwasaki T, Mizutani N, Watano S, Yanagida T, Kawai T (2012) Hydrothermal synthesis of magnetite nanoparticles via sequential formation of iron hydroxide precipitates. J. Exp. Nanosci. 7: 355–365.

[19] Deeng KD, Mohamed AR, Bhatia S (2004) Process optimization studies of structured Cu–ZSM-5 zeolite catalyst for the removal of NO using design of experiments (DOE). Chem. Eng. J. 103: 147–157.

[20] Edrissi M, Hosseinabadi HA (2010) Synthesis of coral-like and spherical nanoparticles of barium titanate using factorial and Taguchi experimental design. Materialwiss. Werkst. 41: 154–160.

[21] Jagdale SC, Patil S, Kuchekar BS (2013) Application of design of experiment for floating drug delivery of tapentadol hydrochloride. Comput. Math. Methods Med. 2013: 625729.

[22] Ma M, Zhang Y, Guo Z, Gu N (2013) Facile synthesis of ultrathin magnetic iron oxide nanoplates by Schikorr reaction. Nanoscale Res. Lett. 8: 16.

[23] Nurdin I, Johan MR, Yaacob II, Ang BC (2014) Effect of nitric acid concentrations on synthesis and stability of maghemite nanoparticles suspension. Sci. World J. 2014: 589479.

[24] Iida H, Takayanagi K, Nakanishi T, Osaka T (2007) Synthesis of Fe_3O_4 nanoparticles with various sizes and magnetic properties by controlled hydrolysis. J. Colloid Interf. Sci. 314: 274–280.

[25] Cornell RM, Schwertmann U (2003) The Iron Oxides: Structure, Properties, Reactions, Occurrences and Uses. Weinheim: Wiley-VCH. pp. 163–164.